

Article

Development of a Radio-Frequency Quadrupole Accelerator for the HL-2A/2M Tokamak Diagnostic System

Shuo Liu ¹, Yaxia Wei ², Yuanrong Lu ^{1,*}, Zhi Wang ¹, Meiyun Han ¹, Tianhao Wei ¹, Yin Xia ¹, Haipeng Li ¹, Shuli Gao ¹ and Pengfei Zheng ^{2,*}

¹ State Key Laboratory of Nuclear Physics and Technology, School of Physics, Peking University, Beijing 100871, China; liushuo@pku.edu.cn (S.L.); wangzhi@pku.edu.cn (Z.W.); hmyoku@pku.edu.cn (M.H.); weitianhao@pku.edu.cn (T.W.); huas22@pku.edu.cn (Y.X.); lih@pku.edu.cn (H.L.); gaoshuli@pku.edu.cn (S.G.)

² Southwestern Institute of Physics, Chengdu 610041, China; weiyaxia@swip.ac.cn

* Correspondence: yrly@pku.edu.cn (Y.L.); zhengpf@swip.ac.cn (P.Z.)

Featured Application: An accelerator-based in situ materials surveillance on a tokamak.

Abstract: In order to figure out the migration and deposition of impurities on the first wall of HL-2A/2M tokamak, Peking University and Southwestern Institute of Physics are co-developing a deuteron RFQ as part of the in situ ion-beam diagnostic for the material. The RFQ, which operates at 162.5 MHz, is designed to accelerate a 10-mA deuteron beam from 40 keV up to 1.5 MeV. Key design considerations and the final design parameters are presented. The RFQ has been conditioned at a 1% duty factor for 80 h at RF cavity power of 55 kW. The specific shunt impedance of the cavity is 221 kΩ·m by measuring the bremsstrahlung spectrum. The intrinsic *Q*-value after the high-power tests measured by the Ring-Down method is 13,780. Beam commissioning has been taken place during the first half of 2021, and the beam measurements include beam current and energy of ²H⁺ ion. A 10 mA ²H⁺ beam was successfully accelerated through the RFQ.

Keywords: beam dynamics; RF conditioning; beam commissioning



Citation: Liu, S.; Wei, Y.; Lu, Y.; Wang, Z.; Han, M.; Wei, T.; Xia, Y.; Li, H.; Gao, S.; Zheng, P. Development of a Radio-Frequency Quadrupole Accelerator for the HL-2A/2M Tokamak Diagnostic System. *Appl. Sci.* **2022**, *12*, 4031. <https://doi.org/10.3390/app12084031>

Academic Editor: Francesco Clementi

Received: 13 March 2022

Accepted: 13 April 2022

Published: 15 April 2022

Publisher's Note: MDPI stays neutral with regard to jurisdictional claims in published maps and institutional affiliations.



Copyright: © 2022 by the authors. Licensee MDPI, Basel, Switzerland. This article is an open access article distributed under the terms and conditions of the Creative Commons Attribution (CC BY) license (<https://creativecommons.org/licenses/by/4.0/>).

1. Introduction

The power supplies through thermonuclear fusion are a promising option to replace fossil fuel as the world's primary energy source in the second half of the 21st century. In the current stage, sustained plasma burning is a critical issue towards the realization of fusion energy [1], for which, impurities should be well diagnosed and controlled so that the risks of burning plasma quenched by the impurities could be moderated. In the past decades, various optical spectrum and numerical simulations have been developed and are used for the studies of impurity transport in tokamak plasma [2,3]. Moreover, ex situ measurements with high precision [4,5] and laser-induced breakdown spectroscopy with the advantage of online analysis [6,7] were widely used to study the deposition of such impurities as well as fuel retention on the first wall and divertor. Great progress has been achieved in the development of the impurity diagnostic technology, except for a trade-off between quantitative analysis and real-time feedback that appeared to be an obstacle to the study of impurity depositions. More recently, an Accelerator-based In situ Materials Surveillance (AIMS) was constructed on the Alcator C-Mod tokamak for plasma-material interaction [8], and the fuel retention was evaluated via nuclear reaction analysis (NRA). In order to figure out the migration and deposition of impurities on the first wall of Huan-Liuqi-2A/2M (HL-2A/2M) tokamak, Peking University (PKU) and Southwestern Institute of Physics (SWIP) are co-developing a deuteron radio-frequency quadrupole (RFQ) accelerator as part of the in situ ion-beam diagnostic for the material.

We aim at a ~MeV deuteron beam into the first wall, which interacts with the surface substance of the wall to produce energetic particles and gamma rays. Then, we can reconstruct the evolution of plasma-facing components' surface compositions by the detected spectroscopy of energetic particles and gamma rays. The deuteron-induced nuclear reactions such as ${}^2\text{H}(\text{d},\text{n}){}^3\text{He}$, ${}^{12}\text{C}(\text{d},\text{p}\gamma){}^{13}\text{C}$, ${}^{14}\text{N}(\text{d},\text{p}\gamma){}^{15}\text{N}$, ${}^{16}\text{O}(\text{d},\text{p}\gamma){}^{17}\text{O}$, ${}^7\text{Li}(\text{d},\text{p}\gamma){}^8\text{Li}$, ${}^9\text{Be}(\text{d},\text{p}\gamma){}^{10}\text{B}$ and ${}^{11}\text{B}(\text{d},\text{p}\gamma){}^{12}\text{B}$ are usually used to diagnose the impurities on plasma-facing components.

The RFQ is a 4-vane room-temperature RFQ, able to accelerate a 10-mA deuteron beam from 40 keV up to 1.5 MeV, operating at 162.5 MHz with a duty factor of 1%. The length of the RFQ is 2.2 m and the calculated RF power consumption is 45 kW. It has been successfully conditioned to the RF power of 55 kW required for deuteron operation, with a sufficient power margin. The beam commissioning demonstrated that the RFQ is performing well with the design parameters.

The paper is organized as follows. Section 2 presents the procedure and criteria adopted for the beam dynamics design of the RFQ. Details of RF conditioning and beam commissioning are presented in Sections 3 and 4, respectively.

2. Beam Dynamics Design

The PARMTEQM [9] code is used to carry out the RFQ dynamics design. The choice of the input beam energy is a trade-off of the RFQ length and the space-charge effects. On the one hand, a low input energy beam makes the RFQ shorter. On the other hand, a higher energy beam can effectively reduce the effect of space charge. Accordingly, we choose 20 keV/u as the input energy for the RFQ design. A high inter-vane voltage results in a high accelerating gradient, which makes the RFQ shorter. However, it requires more RF power dissipation per unit length and increases the risk of RF breakdown. Based on the operational experience of RFQs, we select an inter-vane voltage of 70 kV to ensure the reliable operation of the RFQ. The Peak surface field is one of the most important parameters of the RFQ design. In our design, the peak surface field is 1.52 times the Kilpatrick limit of 13.6 MV/m [10]. Such a low surface electric field is beneficial to maintaining the stability of the RFQ in high-power operation. Another important issue is that the threshold energy of the deuteron breakup reaction is 100 keV [11]. Since this reaction can lead to the activation of the structure due to neutron generation, the beam losses at the high-energy section should be minimized.

An approach is adopted to change the average aperture at the initial cells, which can reduce the difficulty of beam matching from the low energy beam transport (LEBT) into the RFQ [12,13]. In a typical RFQ design, the average aperture of the radial matching section (RMS) is reduced gradually, and the average aperture after the RMS remains constant, as shown in Figure 1. While in the new design, the average aperture after the RMS is larger than that of the typical design.

The matched beam ellipse at the entrance of the RFQ under the two design methods is shown in Figure 2. It can be seen that the matched beam of the new design has a smaller incident angle and a larger envelope.

The final RFQ design parameters as a function of the RFQ cell are given in Figure 3. ϕ_s is the synchronous phase. m is the modulation factor. a is the minimum aperture. W_s is the kinetic energy of the synchronous particles. r_0 is the average aperture. V is the inter-vane voltage. Figure 4 shows the transverse beam envelope and the longitudinal phase space evolution along the RFQ cell according to PARMTEQM. The beam distribution at the exit of the RFQ is shown in Figure 5. A summary of the RFQ parameters is listed in Table 1.

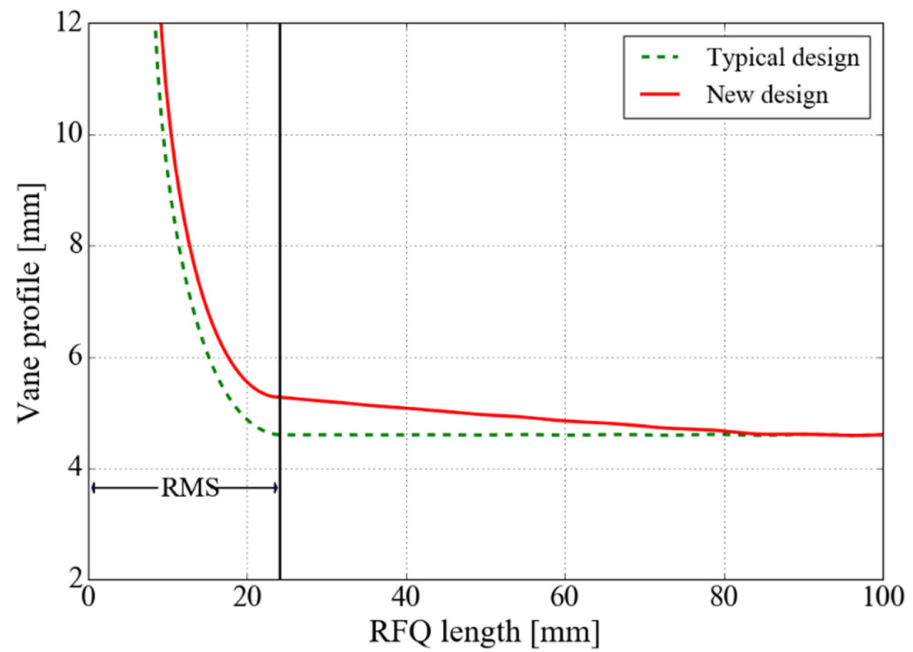


Figure 1. Vane profile at the initial cells under two design methods.

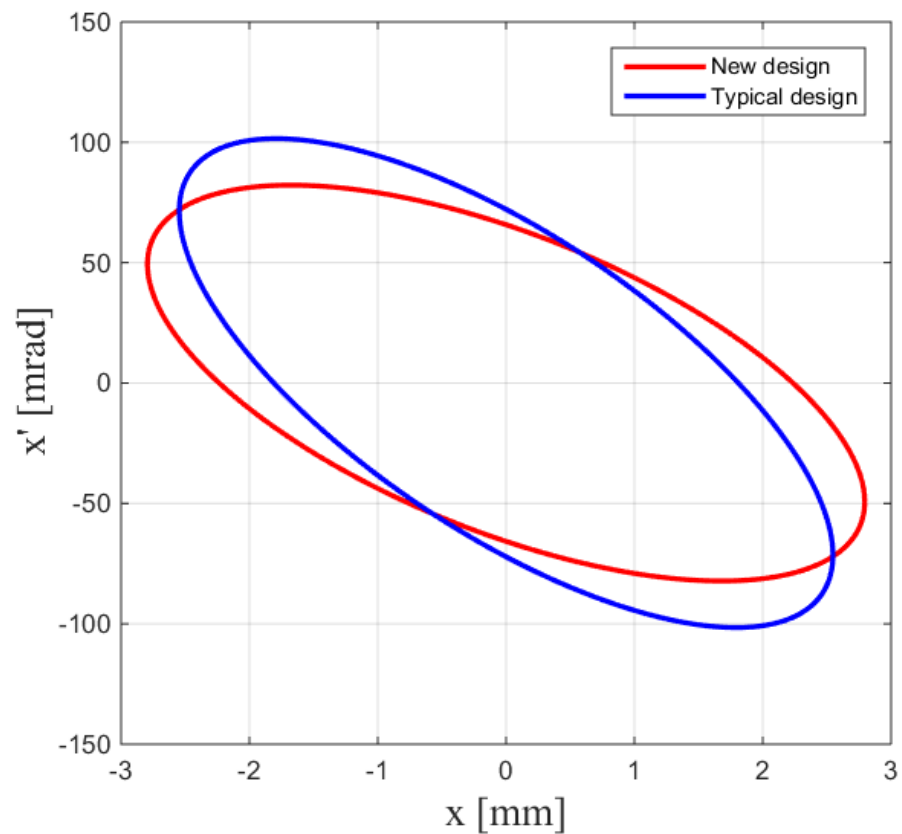


Figure 2. The matched beam ellipse at the entrance of the RFQ under two design methods. New design method (red): $\alpha = 0.75$, and $\beta = 0.0425$ mm/mrad. Typical design method (blue): $\alpha = 0.99$, and $\beta = 0.0353$ mm/mrad.

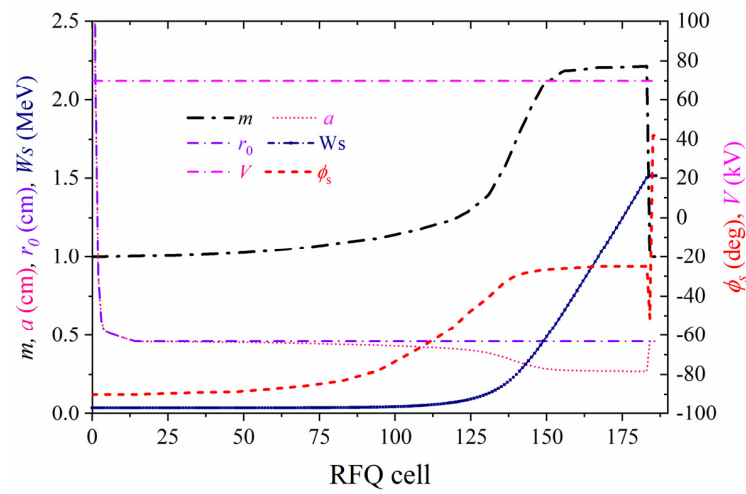


Figure 3. Evolution of the RFQ design parameters along the RFQ cell after optimization.

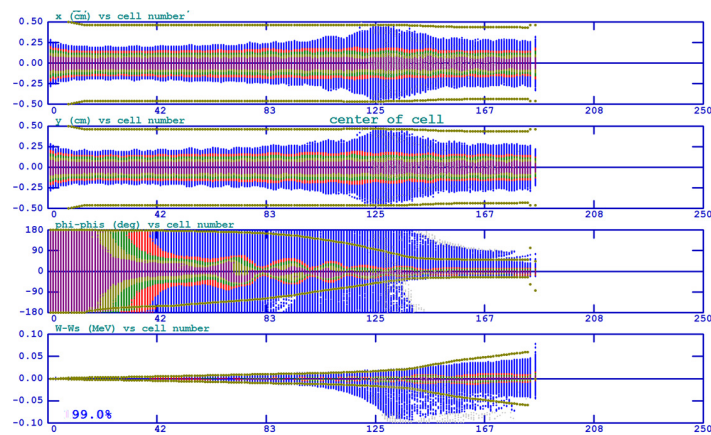


Figure 4. Evolution of beam envelopes along the RFQ cell from PARMTEQM. Plots from top to bottom are the beam profiles in the x and y planes and phase and energy spectrums, respectively.

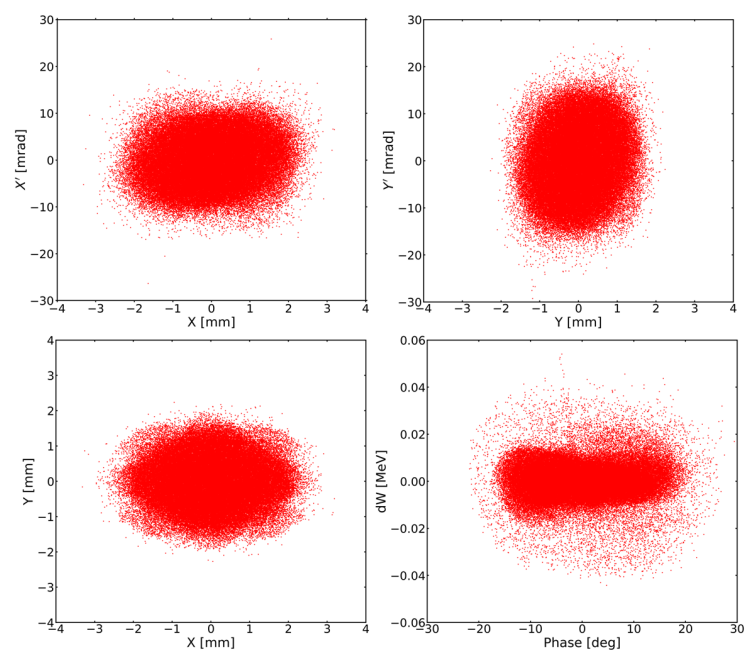


Figure 5. Particles phase-space distribution at the exit of the RFQ.

Table 1. Main physics parameters of the RFQ.

Parameter	Value
Ion species	D ⁺
RFQ type	4-vane
Frequency [MHz]	162.5
Beam current [mA]	10
Input normalized ε_t [$\pi \cdot \text{mm} \cdot \text{mrad}$]	0.20
Input energy [keV]	40
Output energy [MeV]	1.52
Duty cycle [%]	1
Voltage [kV]	70
Length [m]	2.191
Peak field	1.52 kp
Minimum aperture radius [cm]	0.270
Average aperture radius [cm]	0.460
Vane tip radius [cm]	0.345
Synchronous phase	-90° to -25°
Maximum modulation factor	2.2
Output normalized ε_t [$\pi \cdot \text{mm} \cdot \text{mrad}$]	0.208
Output longitudinal normalized ε_l [MeV·deg]	0.060
Transmission efficiency [%]	99.0
Radius of cavity [mm]	173.82
RF power consumption [kW]	45
Specific shunt impedance [$\text{k}\Omega \cdot \text{m}$]	240
Mode separation [MHz]	3.1
Intrinsic Q-value	14,722

3. RF Conditioning

3.1. Coupling Factor for Setup

The RFQ requires a total power of about 71 kW, the cavity power (P_{cav}) is 56 kW (20% redundancy has been considered), the beam power (P_{beam}) is 15 kW. The RF power is fed by a magnetic loop coupler and a 120 kW RF amplifier. According to the definition of the coupling factor, the factor is given by:

$$\beta = \frac{Q_0}{Q_{ext}} = \frac{P_{ext}}{P_{cav}} = \frac{P_{cav} + P_{beam}}{P_{cav}} \quad (1)$$

Therefore, the coupling factor needed to be set as 1.27, and the input reflection coefficient S_{11} is -18.55 dB.

The cavity power was measured by reading the scope amplitude of the RF pick-up (50 Ω impedance). The coupling factor of the pick-up can be measured by a two-port network composed of a coupler and a pick-up, as shown in Figure 6. The coupling factor of the pick-up is given by:

$$\beta_{pickup} = \frac{P_{pickup}}{P_{cav}} \quad (2)$$

The coupling factor $\beta_{pickup1}$ that we measured by the network analyzer is 6.15×10^{-7} , which is -62.2 dB. In the case of neglecting coaxial cable line loss, the dependence of the cavity power on the scope amplitude is given by:

$$P_{cav} = \left(\frac{V_{pp}}{2} \right)^2 \frac{1}{2 \times 50} \times 10^{6.22} \times 10^{-3} \quad (3)$$

where P_{cav} is in kW and V_{pp} is the peak-to-peak voltage of the scope.

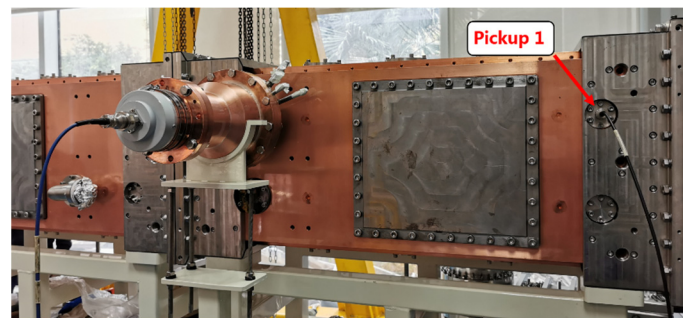


Figure 6. Coupling factor for setup.

3.2. High-Power Tests

The main purpose of the high-power tests is to improve the cavity vacuum through an outgassing process when the cavity is heated after the RF power is loaded and to eliminate the burrs on the inner surface of the cavity through the controlled sparks. Additionally, we also need to calibrate how much RF power can achieve the design inter-vane voltage for the beam commissioning.

The forward and backward power was measured by the directional coupler. We can monitor the spark through the reflected signal and the vacuum gauge, and adjust the frequency of the pulse modulated RF source to minimize the backward power to track the resonance frequency of the cavity.

The RFQ uses 99.9% oxygen-free copper produced by Chinalco Luoyang Copper Processing Co., Ltd. Luoyang, China [14]. The RF conditioning started when the vacuum pressure reached a level below 1.5×10^{-5} Pa. The main difficulty met during the primary RF conditioning is that: the vacuum pressure rises significantly as the cavity power increases, and the worst cavity vacuum reached 9.5×10^{-4} Pa. At first, we suspected that the cavity was not well sealed. This may cause the RF spark and irreversible pollution to the cavity if we continue to increase the cavity power. We performed a leak test on the cavity while maintaining a low level of cavity power, and no leakage of the cavity was found.

As a result of our investigation, we found that this 99.9% oxygen-free copper has the problem of hydrogen adsorption [15]. The most effective way to degas hydrogen on the metal surface is to anneal the metal. Fiberglass heating belts were used to heat the RFQ cavity. Additionally, we also increased the inlet temperature of the RFQ cooling water from 16 °C to 20 °C. During the consecutive seven days, the cavity vacuum slowly improved with RF conditioning at a power of 55 kW. In addition, the reflected signal on the scope was stable and there was almost no spark in the cavity. The log of a 6-h long operation at 55 kW is shown in Figure 7. The cavity power trace was almost constant and the cavity vacuum trace was slow to fall during that time.

Another problem encountered during RF conditioning came from the cooling system of the RFQ. The inlet water temperature of the cooling water cannot be maintained at a certain value, and the inlet water temperature difference reached 3 °C, as shown in Figure 7 (blue trace). Since the RFQ operates at a 1% duty cycle, the heat loss caused by RF power is relatively small. During RF conditioning with a power of 55 kW, we recorded the resonant frequency of the cavity under different cooling water temperatures. The influence of the inlet water temperature on the frequency of the cavity is shown in Figure 8. A new cooling system will be introduced into the RFQ in the future to reduce frequency instability during high-power operations.

After 80 net hours of RF conditioning, a vacuum pressure of 7.5×10^{-6} Pa was achieved without RF power. Although the cavity vacuum was reduced to 3.5×10^{-5} Pa during high-power operation, it still met the requirements of subsequent beam commissioning.

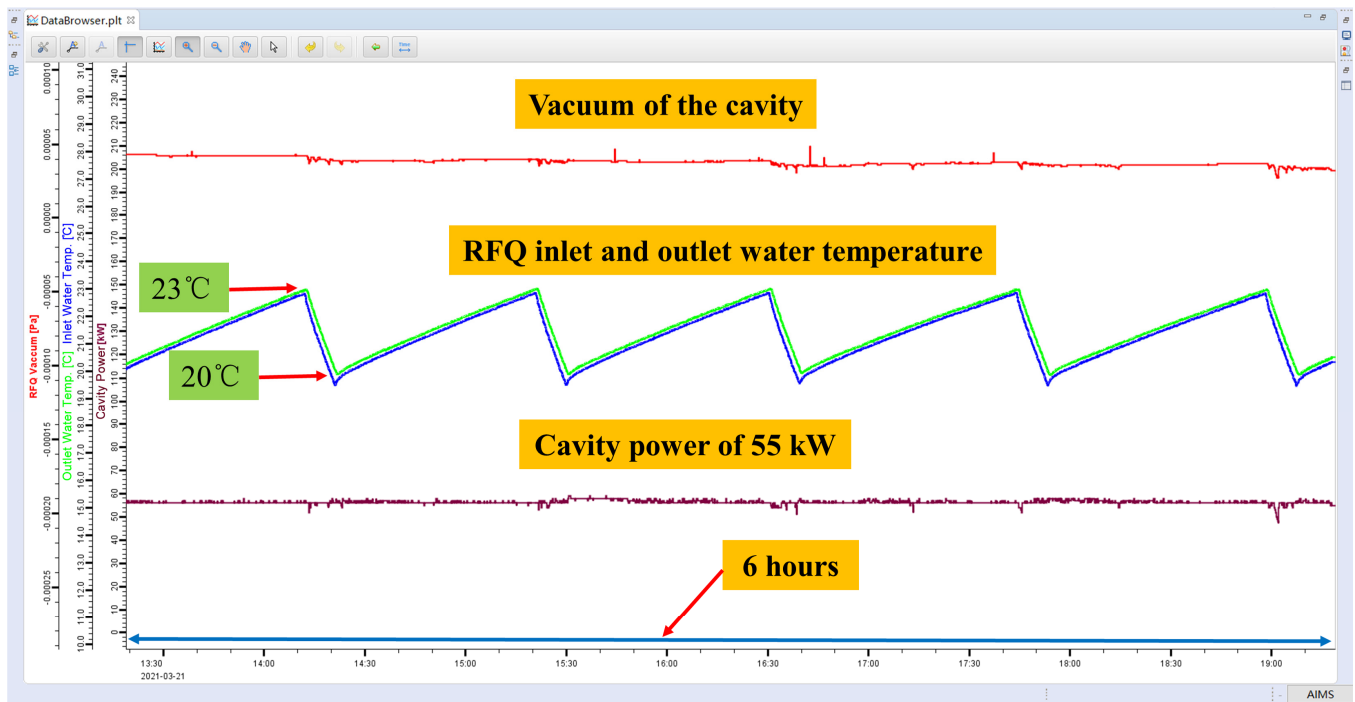


Figure 7. The log of a 6-h long operation without a trip.

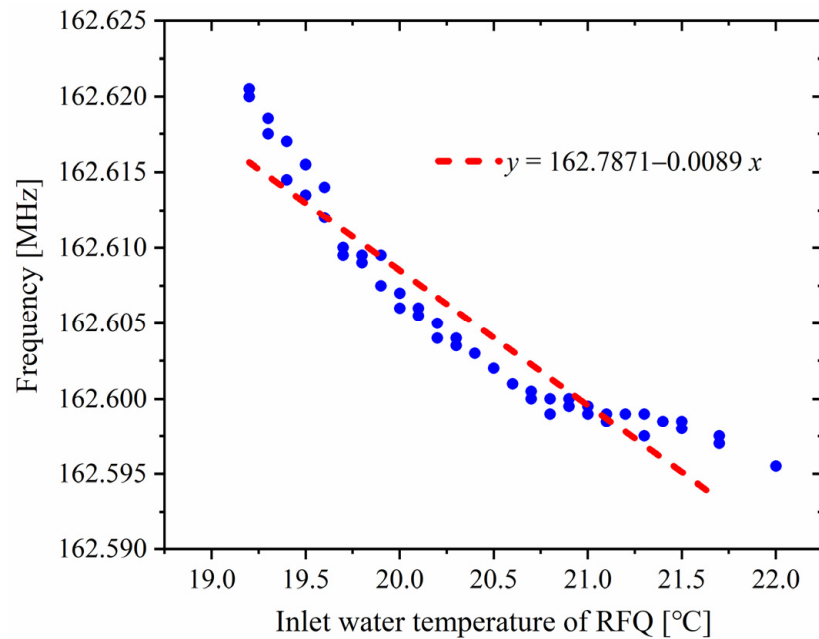


Figure 8. The frequency of the RFQ as a function of inlet water temperature.

3.3. Inter-Vane Voltage Measurement

The inter-vane voltage of RFQ is one of the most important parameters of the cavity. Measurement of the bremsstrahlung X-ray is a useful non-intrusive and precise technique for inter-vane voltage calibration. The bremsstrahlung spectrum originates from the stopping in electrodes of field emission electrons across voltage gaps. X-ray spectra were measured by using a CdTe spectrometer. The spectrometer was calibrated with Am-241 sources, as shown in Figure 9.

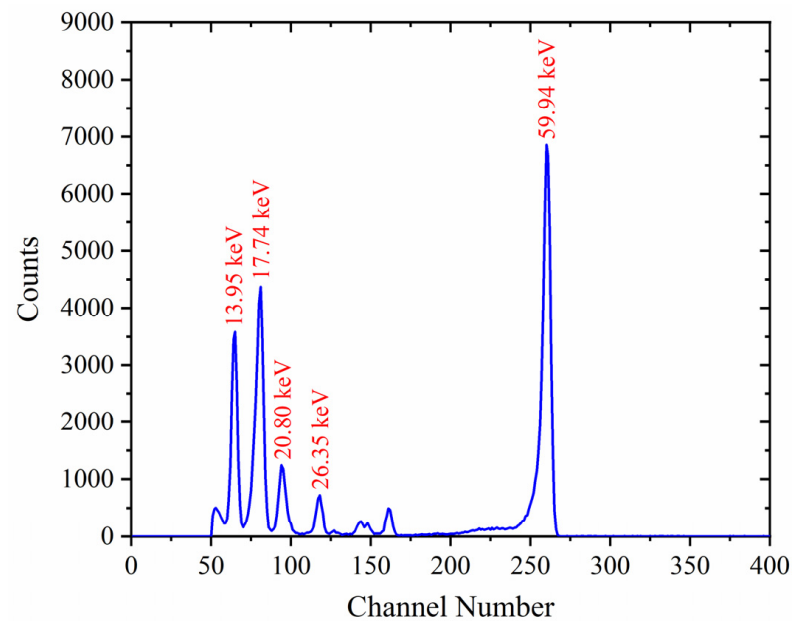


Figure 9. Spectrometer calibration with Am-241.

The quartz window was located in the middle of the cavity. Because the spectrometer cannot directly face the gap between adjacent electrodes in the quadrilateral cavity, the spectrometer and the quartz window were at a 45-degree angle to obtain as many counts as possible, as shown in Figure 10.

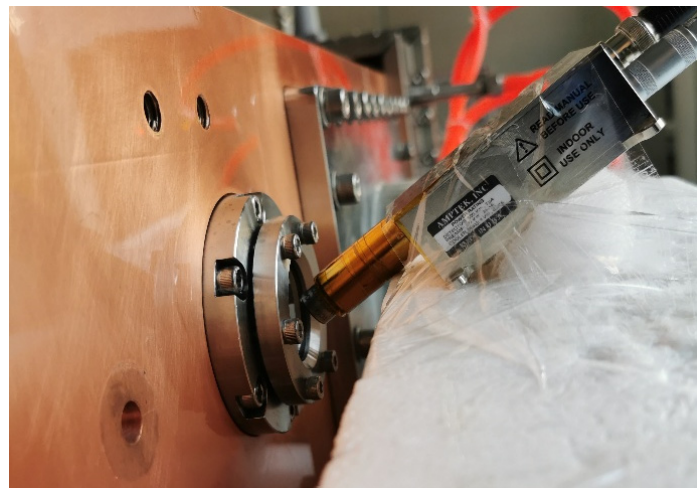


Figure 10. The quartz window and spectrometer.

In the measurement, we used a 1.0 mm thick copper absorber plate to filter out low-energy peaks and backgrounds. A typical 1X-ray spectrum corresponding to the RFQ inter-vane voltage is shown in Figure 11. There are different ways of quantifying the cutoff energy [16–18]. We adopted linear fitting with a beveled edge for the high energy region and took the horizontal intercept as the cutoff energy. The specific shunt impedance is defined as follows:

$$R_s = \frac{V^2}{P/l} \quad (4)$$

where V is the inter-vane voltage, P the power loss, and l the RFQ length.

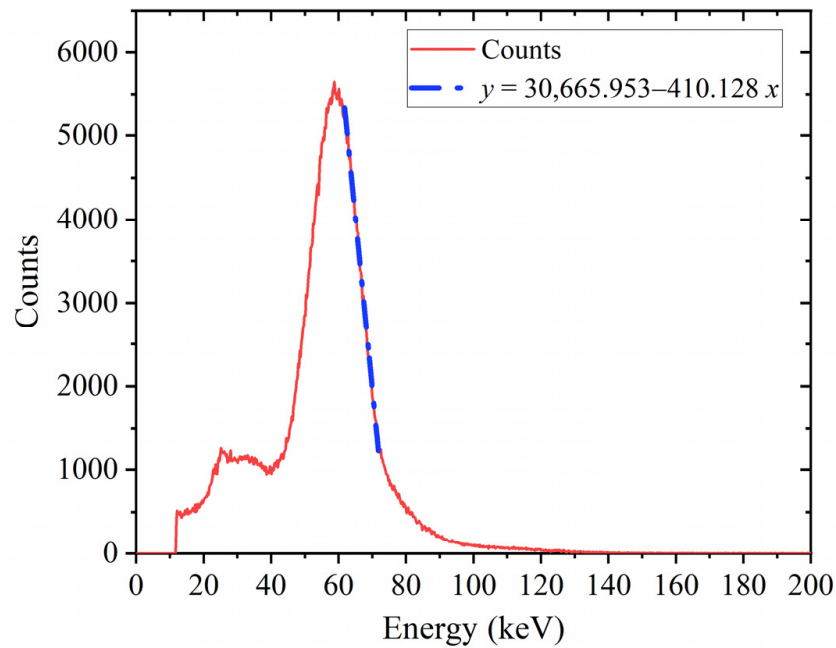


Figure 11. X-ray spectrum corresponding to the 74.8 kV inter-vane voltage (@ 55 kW).

We measured the inter-vane voltage under different cavity powers, as shown in Figure 12. The specific shunt impedance of the RFQ can be deduced from the slope of the linear fitting line ($y = 100.086x$ from Figure 12). The specific shunt impedance is 221 kΩ·m, which is 92% of the simulated value. According to the calculated specific shunt impedance, an inter-vane voltage of 70 kV can be achieved at a cavity power of 48.6 kW.

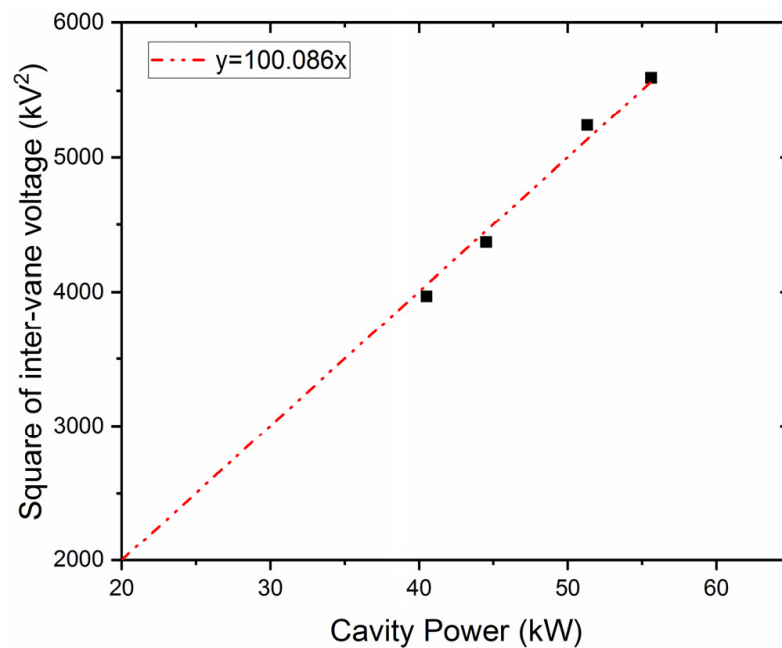


Figure 12. Square of inter-vane voltage as a function of cavity power.

3.4. Measuring Q-Factor with the Ring-Down Method

The ring-down method is a way of measuring the resonator Q-factor. We can obtain the decay time by exponentially fitting the falling edge of the scope amplitude of the cavity power, as shown in Figures 13 and 14.

$$Q_L = \frac{\omega_0 W}{P} \tag{5}$$

where Q_L is the loaded quality factor, $\omega_0 = 2\pi f_0$, f_0 is the resonance frequency, W is the stored energy of the cavity, P is the power loss on the cavity walls.

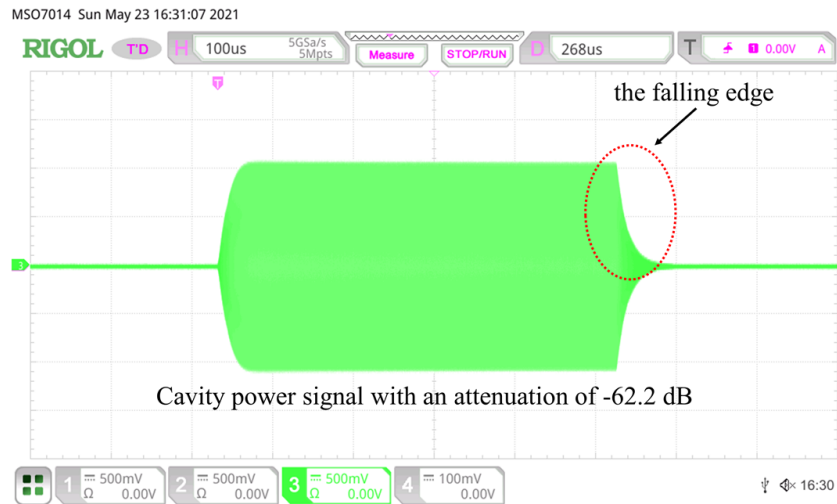


Figure 13. Pickup signal of the RFQ cavity.

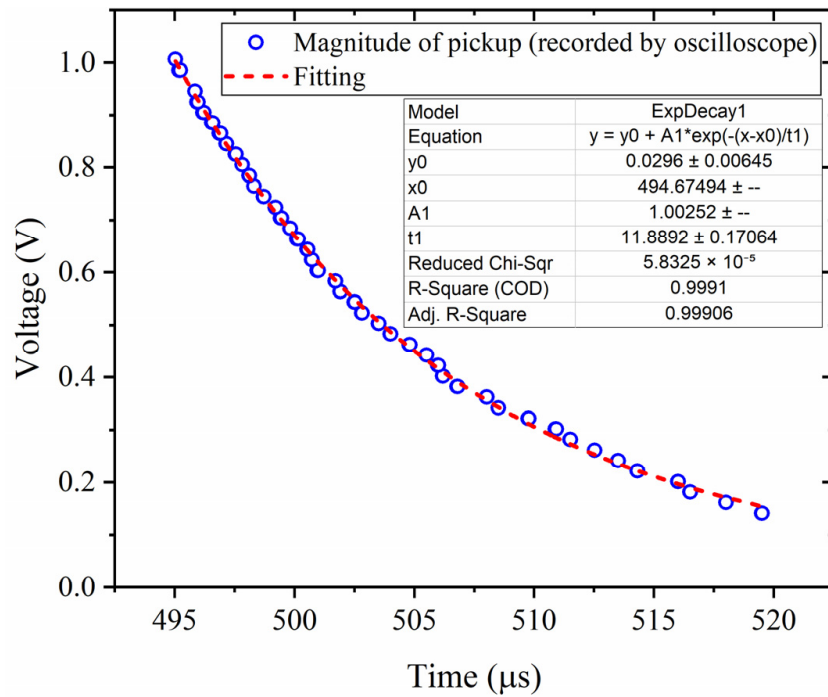


Figure 14. Exponential fitting of decay curve.

Power loss P also can be written as $P = -\frac{dW}{dt} = \frac{\omega_0 W}{Q_L}$. By integrating both sides of the equation separately, we can obtain the equation:

$$W = W_0 \exp\left(-\frac{\omega_0 t}{Q_L}\right) = W_0 \exp\left(-\frac{t}{\tau_L}\right) \quad (6)$$

where $\tau_L = \frac{Q_L}{\omega_0}$, and the voltage $U \propto \sqrt{W}$, then U can be written in the following form:

$$U = U_0 \exp\left(-\frac{t}{2\tau_L}\right) \quad (7)$$

According to the exponential fitting of the decay curve in Figure 13, we can obtain $2\tau_L = (11.89 \pm 0.17) \mu\text{s}$. The loaded quality factor can be expressed as:

$$Q_L = \tau_L \omega_0 = \tau_L \times 2\pi f_0 \quad (8)$$

For our experiment, the resonance frequency f_0 is 162.6055 MHz. Thus, the $Q_L = 6070 \pm 87$. Then the intrinsic Q -value can be calculated to be $13,780 \pm 197$ by:

$$Q_0 = (1 + \beta)Q_L \quad (9)$$

where β is the coupling factor [Equation (1)], which is equal to 1.27.

The intrinsic Q -value after high-power tests is 13,780, which is about 93.6% of the simulated value. The specific shunt impedance by measuring the bremsstrahlung spectrum is 221 k Ω ·m, which is 92% of the simulated value.

After the fabrication and assembly of the RFQ cavity, RF measurements were performed to check the RF properties of the cavity and the quality of the electric field. The intrinsic Q -value after high-power tests is much better than the measurement value of 12,834 in the RF measurements [19], indicating that the high-power tests can improve the conductivity about 6.8% higher of the inner copper surface of the cavity. We compared the measured Q_{meas} and f_{meas} with the simulated value, the required power P_{req} of the cavity is 48.2 kW by:

$$\frac{P_{req}}{P_{sim}} = \frac{Q_{sim}}{Q_{meas}} \cdot \frac{f_{meas}}{f_{sim}} \quad (10)$$

4. Beam Commissioning

The experimental setup for beam commissioning of the RFQ is shown in Figure 15. It consists of a 2.45 GHz electron cyclotron resonance (ECR) ion source, a LEPT system, the RFQ, and a medium energy beam transport (MEBT) section. The LEPT has two solenoids (Solenoid 1 and Solenoid 2) to transport the beam and match it into the RFQ. A pair of steerers (horizontal and vertical) is installed in the middle of each respective solenoid. In order to characterize the beam extracted from the ion source, the diagnostics chamber equipped with a water-cooled diaphragm and faraday cup (FC) is installed between the two solenoids. The water-cooled diaphragm is used to control the intensity and emittance of the beam. The bias voltage of FC is set to -300 V to suppress the secondary electrons (SE). Between the Solenoid 2 and the RFQ, there is a chopper used to control the time structure of the pulse beam, while playing the role of fast protection of the machine. Two beam position monitors (BPMs) are installed after the AC current transformer (ACCT) for beam energy measurement. The extraction voltage of the ion source is fixed at 40 kV to provide the design injection energy of 40 keV for the $^2\text{H}^+$ beam. The low-level RF (LLRF) control is used to synchronize with the timing system of the whole accelerator.

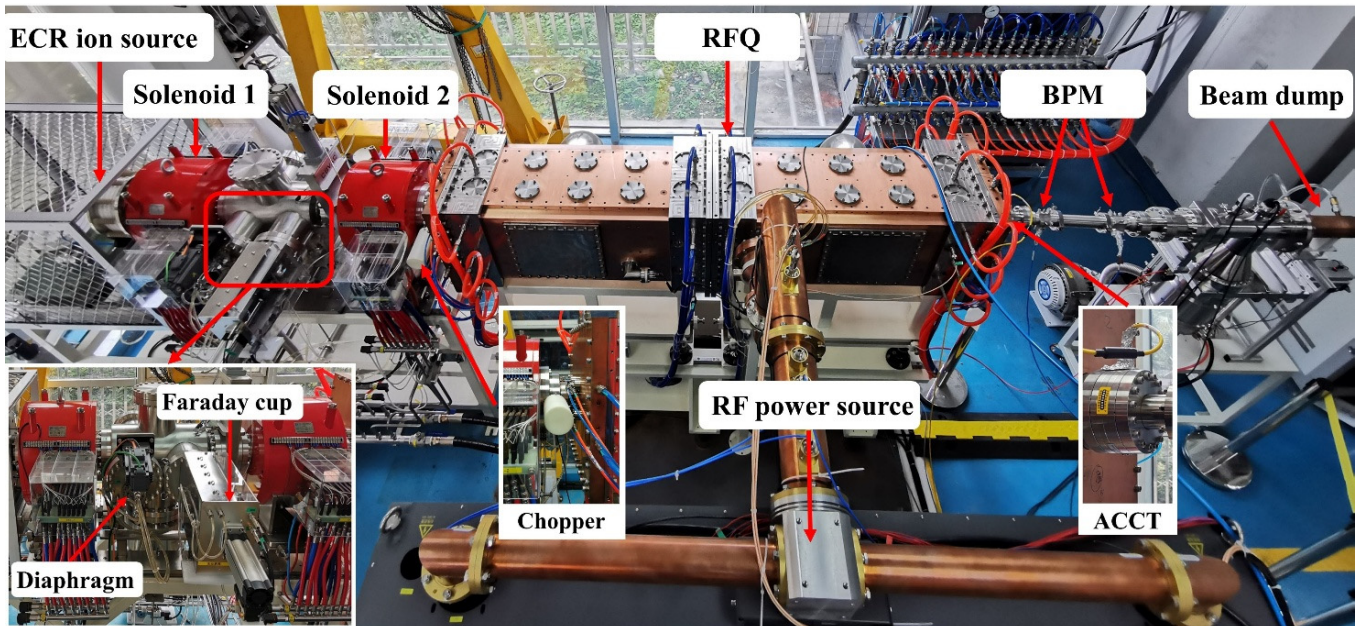


Figure 15. Overview of the RFQ test area.

4.1. Beam Current Measurement

For $^2\text{H}^+$ beam commissioning, we don't care about the transmission efficiency. We are more concerned about whether the beam current at the RFQ exit reaches the design value. After careful optimization of the LEBT solenoids as well as the steerers, we obtained a 10 mA $^2\text{H}^+$ beam at the RFQ exit ACCT, as shown in Figure 16. The current signals from the FC and ACCT are converted to voltage signals through a pure resistance of 500.0 Ω . It was confirmed that a 10 mA $^2\text{H}^+$ beam was successfully accelerated through the RFQ.

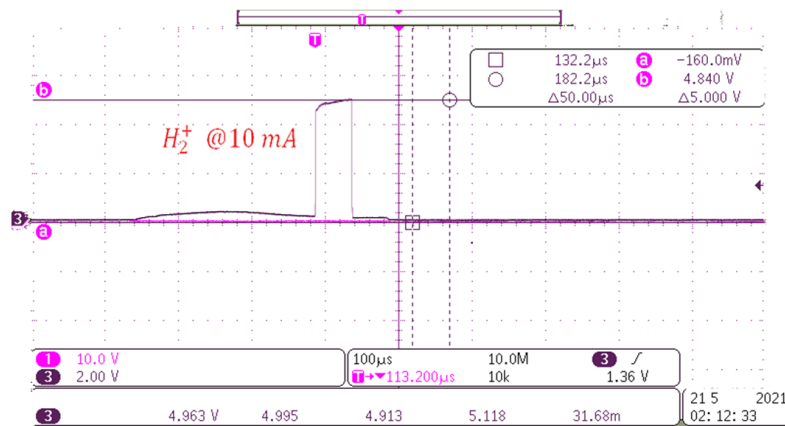


Figure 16. 10 mA $^2\text{H}^+$ beam at the RFQ exit ACCT.

4.2. Beam Energy Measurement

The beam energy was determined by time-of-flight (TOF) using the scope traces from the two BPMs. The TOF principle can be found in [20]. Figure 17 shows the distance between the two BPMs, and Figure 18 shows the corresponding time signals for $^2\text{H}^+$ beam. The flight time of the beam over the distance of 310 mm is $t = \Delta t + nT$, the measured relative time Δt is 1.16 ns, the integer number n of RF periods is equal to 4 and RF period T is 6.16 ns. Therefore, the calculated flight time is 25.80 ns. The velocity and energy of the particles are given by Equations (11) and (12). The error in the energy measurement comes from the measurement of the distance, the cable length, and the resolution of the scope. The

distance error is ± 0.1 mm, and the measurement tolerance of the timing system is ± 200 ps. According to the error transfer formula Equation (13), the energy measurement error of ${}^2\text{H}^+$ is ± 0.024 MeV. We made multiple measurements, and the average output energy of ${}^2\text{H}^+$ is 1.579 ± 0.024 MeV. The beam energy measured by the TOF method agrees well with the designed value.

$$v = \frac{L}{t} \tag{11}$$

$$E = m_0c^2 \left(\frac{1}{\sqrt{1 - \left(\frac{v}{c}\right)^2}} - 1 \right) \tag{12}$$

$$\frac{\Delta N}{N} = \sum \left| \frac{\partial \ln f}{\partial x_i} \right| \Delta x_i \tag{13}$$

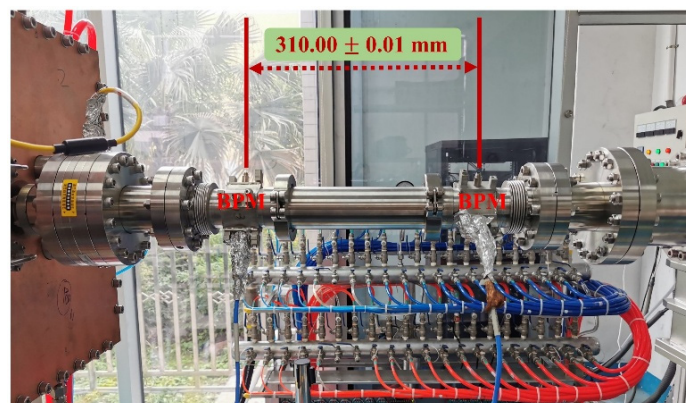


Figure 17. The measured distance of the two BPMs.

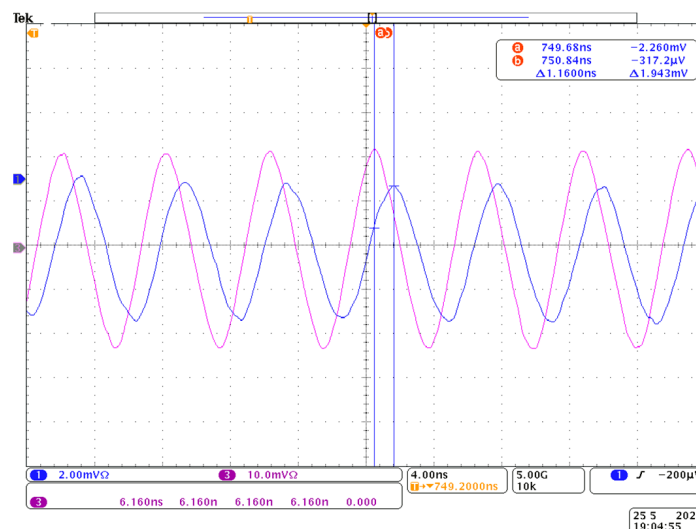


Figure 18. The beam signals detected by the two BPMs.

4.3. Comparison with Other Deuteron RFQs

The main parameters of the deuteron RFQs in the world are listed in Table 2. The SPIRAL2 project located at GANIL in Caen aims at delivering stable and rare isotope beams with intensities. The SPIRAL2 88 MHz RFQ is designed to accelerate light and heavy ions with A/Q from 1 to 3. The power consumption of SPIRAL2 RFQ is 35 kW/m. It has demonstrated a 1.34 mA He^{2+} cw beam.

Table 2. Main parameters of the deuteron RFQs in the world.

Project	Type	Frequency (MHz)	E_{in}/E_{out} (MeV)	Beam Current (mA)	Inter-vane Voltage (kV)	Length (m)	Power (kW)	Status
SPIRAL2 [21–23]	4-vane	88	0.04/1.5	5	100–113	5.08	180	cw 1.34 mA He ²⁺
SARAF [24]	4-rod	176	0.04/2.54	5	56	3.70	186	cw 1.15 mA D ⁺
IFMIF [13,25]	4-vane	175	0.1/5.0	125	79–132	9.8	550	pulse 125 mA D ⁺
CMIF [26]	4-vane	162.5	0.04/3.0	10	65	5.26	120	pulse 7.8 mA ² H ⁺
973-RFQ [27]	window	162.5	0.05/1.0	50	60	1.8	49	cw 1.78 mA ² H ⁺
this work	4-vane	162.5	0.04/1.5	10	70	2.2	45	pulse 10 mA ² H ⁺

Soreq Applied Research Accelerator Facility (SARAF) is a multi-user facility for basic research, medical and biological research, neutron-based non-destructive testing, and radio-pharmaceuticals research [28]. The SARAF 4-rod RFQ was built in 2006, and then RF conditioning and beam commissioning were conducted. Due to the power consumption of up to 65 kW/m when accelerating the D⁺ beam, the operation of the SARAF 4-rod RFQ was extremely difficult [29]. The SARAF 4-rod RFQ was redesigned in 2015 and the power consumption of the upgraded SARAF 4-rod RFQ was reduced to 50 kW/m. The upgraded SARAF 4-rod RFQ has achieved the acceleration of a 1.15 mA deuteron cw beam.

The International Fusion Materials Irradiation Facility (IFMIF) is a fusion neutron source intended for use as a test facility to find and qualify new advanced materials for the plasma-facing components in future fusion reactors. IFMIF RFQ is characterized by very challenging specifications, accelerating a 125-mA cw deuteron beam to 5 MeV within 9.8 m length. The power consumption per unit length is 56 kW/m. A nominal beam current of 125 mA deuteron beam was accelerated up to 5 MeV through the IFMIF RFQ at a duty cycle of 0.1%.

China Material Irradiation Facility (CMIF), which is a compact neutron source with less cost and low-level risk, is designed to provide a material test for fusion reactors. The power consumption per unit length is 23 kW/m. CMIF RFQ has completed the acceleration of a 7.8 mA ²H⁺ beam at the pulse mode.

973-RFQ is collaborating with PKU and the Institute of Modern Physics (IMP). It aims to accumulate experience in the design and fabrication of high-current cw RFQs. 973-RFQ adopts a 4-vane structure with magnetic coupling windows, which is more compact and has sufficient mode separation. The power consumption of 973-RFQ is 27 kW/m. It has successfully accelerated a 1.78 mA ²H⁺ cw beam.

Our RFQ will be used to study the migration and deposition of impurities on the first wall of HL-2A/2M tokamak. The power consumption of our RFQ is 20 kW/m. The low power consumption per unit length is beneficial to the long-term stable operation of the RFQ. A 10 mA ²H⁺ beam was successfully accelerated through our RFQ.

5. Conclusions

In this paper, we have described the beam dynamics, RF conditioning, and beam commissioning of a deuteron RFQ for plasma-material interaction on fusion devices. In the beam dynamics design, the combination of a large aperture radial matching section and weak focusing makes beam matching from the LEBT into the RFQ easy. Beam dynamics parameters were optimized to minimize the emittance growth and also to maximize the beam transmission.

The RFQ was successfully conditioned to the RF power of 55 kW required for deuteron operation, with a sufficient power margin. The inter-vane voltage was calibrated using an X-ray energy measurement technique. An inter-vane voltage of 70 kV can be achieved at a cavity power of 48.6 kW. The intrinsic Q -value measured by the Ring-Down method after high-power tests is 13,780.

The beam commissioning with a $^2\text{H}^+$ beam demonstrated that the RFQ is performing well with the design parameters. A 10 mA $^2\text{H}^+$ beam was successfully accelerated up to 1.5 MeV through the RFQ in May 2021. The acceleration of the D^+ beam is programmed to begin as soon as we obtain the safety authority's authorization.

Author Contributions: Conceptualization, P.Z. and Y.L.; methodology, S.L.; software, S.L.; validation, S.L., M.H. and T.W.; formal analysis, Y.X.; investigation, S.L.; resources, Y.W.; data curation, Z.W.; writing—original draft preparation, S.L.; writing—review and editing, P.Z.; visualization, H.L.; supervision, S.G.; project administration, P.Z.; funding acquisition, P.Z. All authors have read and agreed to the published version of the manuscript.

Funding: This research was funded by the National Key Research and Development Program of China (Grant No. 2017YFE0301306).

Institutional Review Board Statement: Not applicable.

Informed Consent Statement: Not applicable.

Data Availability Statement: The data presented in this study are available on request from the corresponding author.

Acknowledgments: The primary author, Shuo Liu, would like to thank all the partner labs staff for their deep involvement in the project.

Conflicts of Interest: The authors declare no conflict of interest.

References

1. National Academies of Sciences, Engineering, and Medicine. *Final Report of the Committee on a Strategic Plan for U.S. Burning Plasma Research*; National Academies Press: Washington, DC, USA, 2019.
2. Dong, C.; Morita, S.; Feng, L.; Zhang, K.; Zheng, D.; Cui, Z.; Sun, P.; Fu, B.; Lu, P.; Shi, Z.; et al. Space-resolved extreme ultraviolet spectrometer for impurity diagnostics in HL-2A. *Fusion Eng. Des.* **2020**, *159*, 111785. [[CrossRef](#)]
3. Hitzler, F.; Wischmeier, M.; Reimold, F.; Coster, D.P. the ASDEX Upgrade Team Impurity transport and divertor retention in Ar and N seeded SOLPS 5.0 simulations for ASDEX Upgrade. *Plasma Phys. Control. Fusion* **2020**, *62*, 085013. [[CrossRef](#)]
4. Rudakov, D.L.; Wong, C.P.C.; Litnovsky, A.; Wampler, W.R.; Boedo, J.A.; Brooks, N.H.; Fenstermacher, M.E.; Groth, M.; Hollmann, E.M.; Jacob, W.; et al. Overview of the recent DiMES and MiMES experiments in DIII-D. *Phys. Scr.* **2009**, *2009*, 014007. [[CrossRef](#)]
5. Ding, R.; Pitts, R.; Borodin, D.; Carpentier, S.; Ding, F.; Gong, X.; Guo, H.; Kirschner, A.; Kocan, M.; Li, J.; et al. Material migration studies with an ITER first wall panel proxy on EAST. *Nucl. Fusion* **2015**, *55*, 023013. [[CrossRef](#)]
6. Zlobinski, M.; Philipps, V.; Schweer, B.; Huber, A.; Stoschus, H.; Brezinsek, S.; Samm, U.; TEXTOR team. In situ measurements of fuel retention by laser induced desorption spectroscopy in TEXTOR. *Phys. Scr.* **2011**, *2011*, 014027. [[CrossRef](#)]
7. Li, C.; Feng, C.-L.; Oderji, H.Y.; Luo, G.-N.; Ding, H.-B. Review of LIBS application in nuclear fusion technology. *Front. Phys.* **2016**, *11*, 114214. [[CrossRef](#)]
8. Hartwig, Z.S.; Barnard, H.S.; Lanza, R.C.; Sorbom, B.N.; Stahle, P.W.; Whyte, D.G. An in-situ accelerator-based diagnostic for plasma-material interactions science on magnetic fusion devices. *Rev. Sci. Instrum.* **2013**, *84*, 123503. [[CrossRef](#)] [[PubMed](#)]
9. Crandall, K.R.; Wangler, T.P.; Young, L.M.; Billen, J.H.; Neuschaefer, G.H.; Schrage, D.L. *RFQ Design Codes*; LA-UR-96-1836; Los Alamos National Laboratory: Los Alamos, NM, USA, 2005.
10. Kilpatrick, W.D. Criterion for Vacuum Sparking Designed to Include Both rf and dc. *Rev. Sci. Instruments* **1957**, *28*, 824–826. [[CrossRef](#)]
11. Fu, Q.; Zhu, K.; Lu, Y.R.; Easton, M.J.; Gao, S.L.; Wang, Z.; Jia, F.J.; Li, H.P.; Gan, P.P.; He, Y. Design and cold model experiment of a continuous-wave deuteron radio-frequency quadrupole. *Phys. Rev. Accel. Beams* **2017**, *20*, 120101. [[CrossRef](#)]
12. Young, L.M. Simulations of the LEDA RFQ 6.7-MeV accelerator. In Proceedings of the 1997 Particle Accelerator Conference (PAC1997), Vancouver, BC, Canada, 12–16 May 1997; pp. 2752–2754.
13. Comunian, M.; Pisent, A. Beam dynamics redesign of IFMIF-EVEDA RFQ for a larger input beam acceptance. In Proceedings of the 2011 International Particle Accelerator Conference (IPAC2011), San Sebastian, Spain, 4–9 September 2011; pp. 670–672.
14. Available online: <http://www.chalcu.com> (accessed on 12 March 2022).
15. Nordlander, P.; Holloway, S.; Nørskov, J. Hydrogen adsorption on metal surfaces. *Surf. Sci.* **1984**, *136*, 59–81. [[CrossRef](#)]
16. Zhukov, A.P. SNS RFQ Voltage measurements using X-ray spectrometer. In Proceedings of the 2016 International Beam Instrumentation Conference (IBIC2016), Barcelona, Spain, 11–15 September 2016; pp. 154–156.
17. Duke, J.P.; Letchford, A.P.; Findlay, D.J.S. Measurements of RF cavity voltages by X-ray spectrum measurements. In Proceedings of the 20th International Linear Accelerator Conference (LINAC2000), Monterey, CA, USA, 21–25 August 2000; pp. 164–165.

18. Ostroumov, P.N.; Barcikowski, A.; Clifft, B.; Rusthoven, B.; Sharma, S.; Sharamentov, S.I.; Toter, W.F.; Rathke, J.W.; Vinogradov, N.E.; Schrage, D.L. High power test of a 57-MHz CW RFQ. In Proceedings of the 23rd International Linear Accelerator Conference (LINAC2006), Knoxville, TN, USA, 21–25 August 2006; pp. 767–769.
19. Liu, S.; Bai, Q.; Wei, Y.; Lu, Y.; Wang, Z.; Han, M.; Li, H.; Tan, Q.; Wei, T.; Xia, Y.; et al. RF design and tuning of a deuteron RFQ for detecting impurity deposition on a tokamak. *J. Instrum.* **2022**, *17*, P01030. [[CrossRef](#)]
20. Bozzolan, M. BPM time of flight measurements for setting-up the RF cavities of the CERN Linac4. In Proceedings of the 29th Linear Accelerator Conference (LINAC2018), Beijing, China, 16–21 September 2018; pp. 879–881.
21. Ferdinand, R.; Congretel, G.; Curtioni, A.; Delferriere, O.; France, A.; Leboeuf, D.; Thinel, J.; Toussaint, J.; Di Giacomo, M. SPIRAL2 RFQ design. In Proceedings of the 9th European Particle Accelerator Conference (EPAC2004), Lucerne, Switzerland, 5–9 July 2004; pp. 2026–2028.
22. Ferdinand, R.; Bernaudin, P.E.; Bertrand, P.; Di Giacomo, M.; Ghribi, A.; Franberg, H.; Kamalou, O. Commissioning of SPIRAL2 cw RFQ and linac. In Proceedings of the 8th International Particle Accelerator Conference (IPAC2017), Copenhagen, Denmark, 14–19 May 2017; pp. 2462–2465.
23. Di Giacomo, M.; Ferdinand, R.; Franberg, H.; Lagniel, J.M.; Normand, G.; Desmons, M.; Galdemard, P.; Lussignol, Y.; Piquet, O.; Sube, S. RF commissioning of the SPIRAL2 RFQ in cw mode and beyond nominal field. In Proceedings of the 10th International Particle Accelerator Conference (IPAC2019), Melbourne, Australia, 19–24 May 2019; pp. 2804–2806.
24. Weissman, L.; Perry, A.; Bechtold, A.; Berkovits, D.; Kaizer, B.; Luner, Y.; Niewieczeral, P.; Rodnizki, J.; Silverman, I.; Shor, A.; et al. Installation, high-power conditioning and beam commissioning of the upgraded SARAF 4-rods RFQ. *J. Instrum.* **2018**, *13*, T05004. [[CrossRef](#)]
25. Akagi, T.; Bellan, L.; Bolzon, B.; Cara, P.; Carin, Y.; Chauvin, N.; Comunian, M.; Dzitko, H.; Fagotti, E.; Harrault, F.; et al. Commissioning of high current H⁺/D⁺ ion beams for the prototype accelerator of the International Fusion Materials Irradiation Facility. *Rev. Sci. Instrum.* **2020**, *91*, 023321. [[CrossRef](#)] [[PubMed](#)]
26. Dou, W.-P.; Chen, W.-L.; Wang, F.-F.; Wang, Z.-J.; Li, C.-X.; Wu, Q.; Wang, C.; Wang, W.-S.; Jia, H.; Zhang, P.; et al. Beam dynamics and commissioning of CW RFQ for a compact deuteron–beryllium neutron source. *Nucl. Instruments Methods Phys. Res. Sect. A: Accel. Spectrometers, Detect. Assoc. Equip.* **2018**, *903*, 85–90. [[CrossRef](#)]
27. Gan, P.P.; Zhu, K.; Fu, Q.; Li, H.P.; Easton, M.J.; Tan, Q.Y.; Liu, S.; Gao, S.L.; Wang, Z.; Lu, Y.R.; et al. Development and beam commissioning of a continuous-wave window-type radio-frequency quadrupole. *Phys. Rev. Accel. Beams* **2019**, *22*, 030102. [[CrossRef](#)]
28. Nagler, A.; Mardor, I.; Berkovits, D.; Dunkel, K.; Pekeler, M.; Piel, C.; vom Stein, P.; Vogel, H. Status of the SARAF project. In Proceedings of the 23rd International International Linear Accelerator Conference (LINAC2006), Knoxville, TN, USA, 21–25 August 2006; pp. 168–170.
29. Berkovits, D. The SARAF accelerator commissioning. In Proceedings of the Seminar at FNAL, Batavia, NY, USA, 10 February 2011.